Detergent structure in tetragonal crystals of OmpF porin

E Pebay-Peyroula[1,2], RM Garavito[3,4], JP Rosenbusch[3], M Zulauf[5,6†] and PA Timmins[1*]

[1]Institut Laue-Langevin, 156 X, 38042 Grenoble Cedex 9, France, [2]Institut de Biologie Structurale/Université Joseph Fourier, 41 Avenue des Martyrs, 38027 Grenoble Cedex, France, [3]Biozentrum, Klingelbergstr. 70, CH-4056 Basel, Switzerland, [4]Dept. of Biochemistry and Molecular Biology, University of Chicago, 920 East 58th Street, Chicago, IL 60637, USA, [5]EMBL, c/o ILL, BP 156, 38042 Grenoble Cedex 9, France and [6]F Hoffmann-La Roche, PRPS 65-509, CH-4002 Basel, Switzerland

Background: The high-resolution structures of five porins have been solved by X-ray crystallography including the trigonal crystal form of the trimeric OmpF porin from *Escherichia coli*. In an accompanying article, the structure of the tetragonal form of OmpF porin is presented. In contrast to the trigonal crystal form, the protein surfaces normally in contact with lipids in the membrane are exposed and interact with amphiphiles in the tetragonal crystal. Thus, the tetragonal form can be used to investigate protein–detergent interactions.

Results: Using single-crystal neutron diffraction studies and two different detergents (one of them deuterated in its hydrophobic moiety), details of the amphiphile–protein interactions are revealed. Detergent molecules bind to the so-called hydrophobic zone that surrounds the OmpF porin trimer and which is exposed to lipid in the native environment. The aromatic rings on both sides of the hydrophobic zone coincide with the boundary between non-polar and polar moieties of the detergents.

Conclusions: In the tetragonal crystal form of OmpF porin, the membrane-exposed area is accessible from the aqueous solution. It is coated by a film of detergent molecules, which presumably mimics the interactions of the protein with lipids in the biological membrane. In the trigonal form, protein–protein interactions predominate in the hydrophobic zone. These may reflect the tight interactions between trimers that are observed in the biological membrane.

Structure 15 October 1995, **3**:1051–1059
Key words: crystal packing, detergent structure, neutron diffraction, porin

Introduction

The structures of relatively few membrane proteins have been solved to high resolution (<3 Å) by X-ray crystallography. To date, these have been limited to reaction centers [1,2] and porins from photosynthetic bacteria [3,4], and porins from *Escherichia coli* [5,6]. Recently, the light-harvesting complex from *Rhodopseudomonas acidophilia* has been added to this list [7]. The OmpF porin from *E. coli* was the first membrane protein to yield large, well-ordered three-dimensional crystals amenable to X-ray analysis [8,9], but its structure could be solved only by molecular replacement [10] using the trigonal crystal form as a model [5]. Because no detailed knowledge of protein–lipid interactions exists, the structure of the tetragonal form is particularly interesting. In the tetragonal form, the protein surface buried in the membrane is accessible to the detergent solution, and hence the interactions of the amphiphiles used to solubilize the protein can be studied. Clearly, this is also significant for understanding the process of crystallization. Porin loses its directional function when crystallized. This may be caused by a non-membrane-like arrangement and loose packing in the unit cell [11], by an antiparallel orientation of the trimers [5], or by poor order in a seemingly membrane-like arrangement (as observed in the hexagonal crystal form [9]). Therefore, establishing the native state of channel proteins in crystals is of particular interest. Although a well-ordered detergent molecule was observed to be bound per monomer in both the trigonal and tetragonal crystal forms of OmpF [5,10], and less well-defined density was observed in two other porins [3,4], no density attributable to extensive detergent domains was found.

The only available technique for studying the structure of disordered detergent in membrane proteins is neutron diffraction [12,13], whereby the individual components (proteins and amphiphiles) may be visualized by contrast variation (substitution of D_2O for H_2O), a technique commonly used in small-angle scattering [14]. The contrast can also be manipulated by specific deuteration of either or both components (i.e. protein and detergent). This technique has previously been used to study the detergent in crystals of reactions centers [15,16].

In this paper we describe the detergent structure of OmpF porin with β-octyl glucoside (βOG). (Crystals are of the same form as those for which the high-resolution structure of the protein is described in [10]). We also describe the structure in the presence of a different detergent, d_{10}-decyl-*N*,*N*′-dimethyl amine oxide (C_{10}DAO), which has been partially deuterated in its hydrophobic moiety, in order to increase the contrast between protein and detergent.

*Corresponding author. †Deceased 17 June 1995.

 ISSN 0969-2126

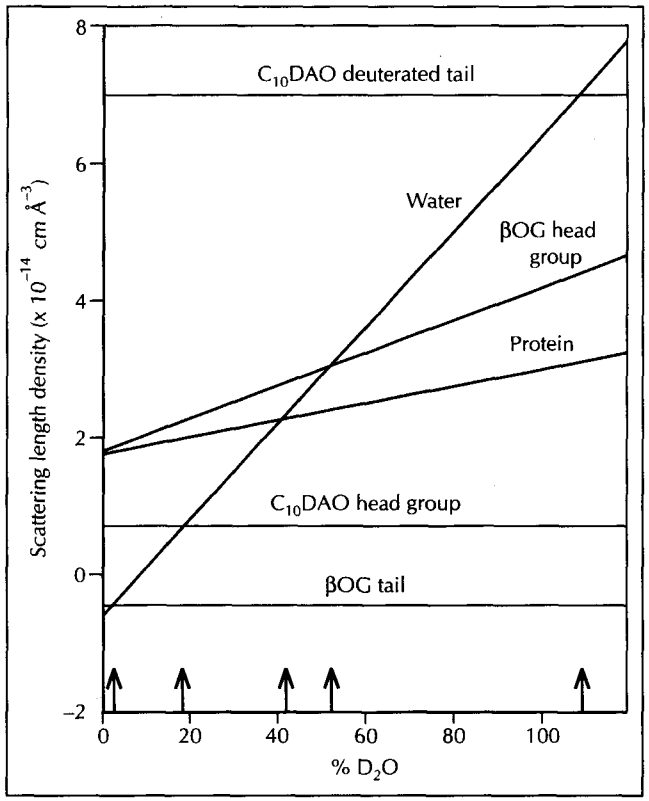

Fig. 1. Calculated scattering-length densities as a function of D_2O concentration are plotted for water, a typical protein, the protonated head group and deuterated tail of C_{10}DAO and the protonated head group and protonated tail of βOG. The volumes of heads and tails used in the calculations for C_{10}DAO are 81 $Å^3$ and 296.4 $Å^3$ respectively and for βOG are 180.3 $Å^3$ and 236.7 $Å^3$ respectively [12]. The matching points (D_2O concentrations at which the contribution of a particular moiety to the diffraction is minimized) are marked by arrows on the abscissa. The match point for the C_{10}DAO deuterated tail is at 110% D_2O, which has no physical meaning but corresponds to an inaccessible contrast.

Results and discussion

Maps at different contrasts

The scattering-length densities and hence the contrast of head groups and tails are significantly different for both C_{10}DAO and βOG (Fig. 1). Whether or not one can distinguish between them in neutron scattering density maps depends on the resolution of the data and the extent to which they form spatially distinct domains. If the head group domains or the tail domains are large relative to the resolution, they should be visible separately. If the detergent region is considered as a single domain, then the scattering density will be the mean calculated over the whole detergent molecule. In fact, the agreement factor (R) between observed and calculated structure factors (F) calculated from the protein alone is a minimum for 3% D_2O in the case of βOG and a virtual 110% D_2O (Fig. 1) in the case of C_{10}DAO (Table 1). This indicates that the protein contribution is predominant in the diffraction patterns obtained at 3% D_2O for βOG and 110% D_2O for C_{10}DAO, whereas the detergent contribution is matched out. These match points are close to those of the tail domains, indicating that the contributions of the hydrophobic tail regions are predominant in the neutron diffracted intensities.

The scattering-length densities of the various components of the crystals are shown in Figure 1. From this we can see the contrast of each component as a function of the deuterium content of the water. Neutron scattering density maps were calculated for D_2O contents of 19% and 40% in the case of C_{10}DAO crystals. At 19% D_2O the head groups are not visible, whereas the protein and deuterated decyl moieties can be seen at intermediate and high positive contrasts, respectively. Similarly, maps for βOG were calculated for solvent contents of 40% and 100% D_2O and reveal the hydrophobic tails at 40% D_2O and both protein and detergent at high negative contrast at 100% D_2O. The maps calculated from the best estimate of structure factors (BESF) procedure (see the Materials and methods section) for C_{10}DAO–porin at two different D_2O concentrations are shown in Figure 2. The 40% D_2O map (Fig. 2a,b) shows a ring of striking high density around the porin trimer, which probably arises from the hydrophobic tails of the detergent. The 110% D_2O map (Fig. 2c) shows not only the protein density but also density at about 15–18 Å from the trimer surface which may correspond to the amine oxide head groups. Maps at 100% D_2O for the βOG detergent are displayed in Figure 3a,b. The annulus of density around the porin trimer is seen to be very similar to that found for C_{10}DAO.

Table 1. Analysis of the detergent model: R factors and mean phase errors.

Detergent	C_{10}DAO				βOG			
Contrast (%) $[D_2O]/[D_2O]+[H_2O]$	0	35	70	100	0	25	60	100
R factor* (%) [protein]	66.1	64.1	52.0	41.4†	31.1	47.4	64.3	67.7
R factor (%) [protein+tail, intermediate model]	39.0	33.2	32.5	40.7	30.9	36.9	37.3	41.4
R factor (%) [protein+tail, final model]	32.9	28.7	33.7	41.2	30.8	35.6	30.0	31.5
R factor (%) [protein+tail+head group, final model]	31.9	28.7	30.7	34.3	–	–	–	–
Mean phase errors (°) [final model]	35.0	34.8	31.4	30.0	25.9	29.7	32.8	29.2

*R factors (%) are calculated as $\Sigma|F_{obs}-F_{calc}|/\Sigma F_{obs}$, where the sum is weighted using the σ_{obs}. The sum is over the reflections with $F>2\sigma$, over the whole resolution range (up to 16 Å). The F_{calc} is calculated for several models as indicated in the table. The mean phase errors are estimated during the phase calculations in the best estimate of structure factors (BESF) algorithm. †R as a function of resolution: 18.4% (d>50 Å), 29.6% (30 Å<d<50 Å) and 50.5% (d<30 Å).

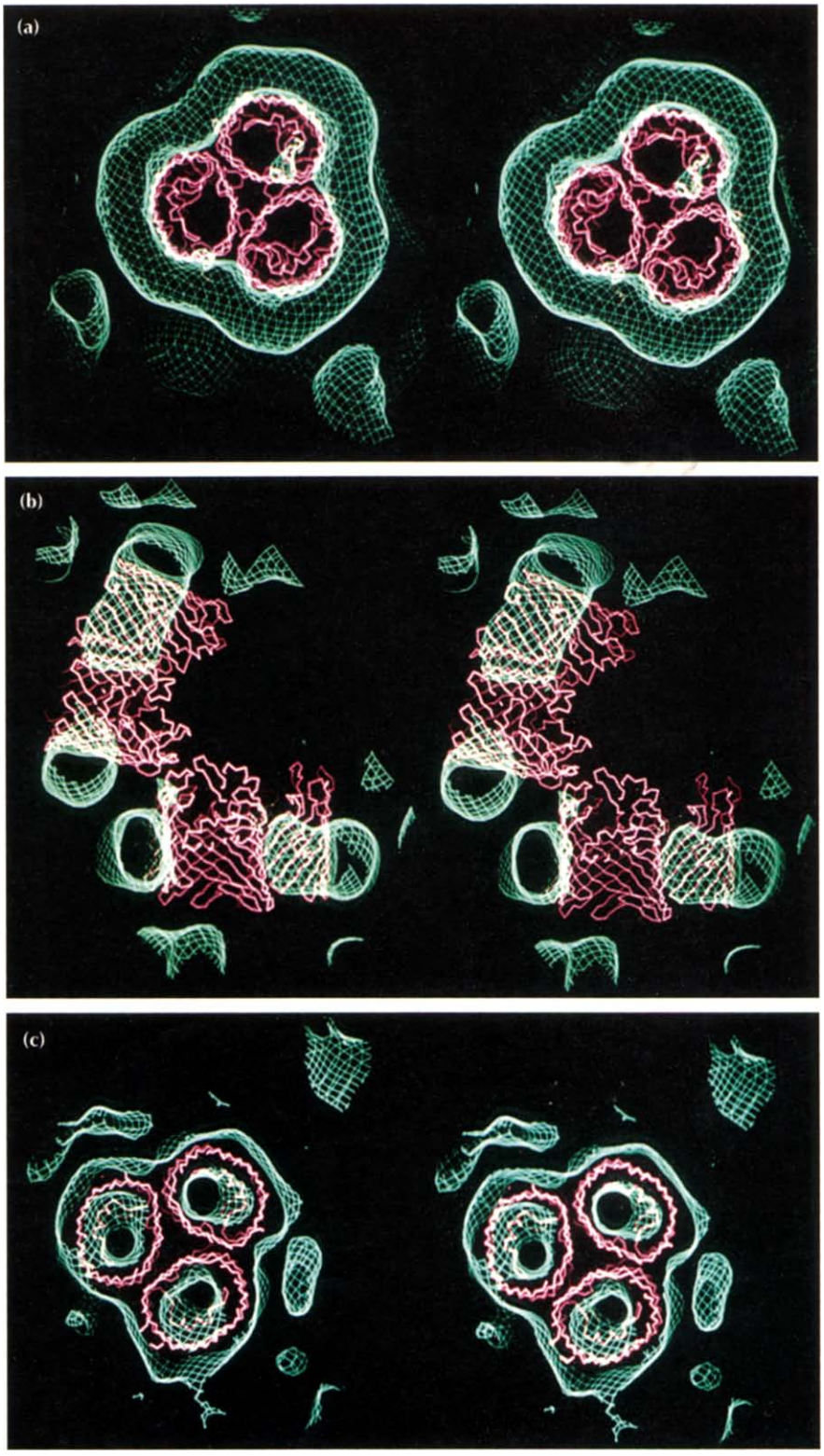

Fig. 2. Stereoviews of the scattering-length density map of C_{10}DAO–porin. Two views are shown at 40% D_2O, where the protein is contrast matched, parallel **(a)** and perpendicular **(b)** to the trimer threefold axis. These maps are contoured at positive contrast so that the density encloses 24% of the cell volume and therefore represents the deuterated tails of the detergent molecules. The porin trimers are represented by their Cα traces (pink) obtained from the X-ray structure. **(c)** C_{10}DAO–porin in 110% D_2O (see the Materials and methods section). At this contrast, the deuterated detergent tails are contrast matched and the protein and *N,N'*-dimethyl amine oxide head groups are visible at negative contrast. The map is contoured so as to enclose 30% of the cell volume of which 26% would be protein and 4% detergent head group.

Model building

In order to improve the quality of these maps, the density assigned as detergent was modeled as a function of its volume fraction in the unit cell and using solvent flattening on the aqueous phase (see the Materials and methods section). The protein density was masked and unaltered in the modeling procedure.

Modeling of the detergent was from 19% and 40% D_2O maps for C_{10}DAO and 40% or 100% D_2O for βOG. The amount of detergent in the crystal is not known accurately; radioactive labeling has indicated a detergent content of between 20% and 36% of the cell volume [9]. The best modeling results (in terms of lowest R factor) were obtained with the hydrophobic tails

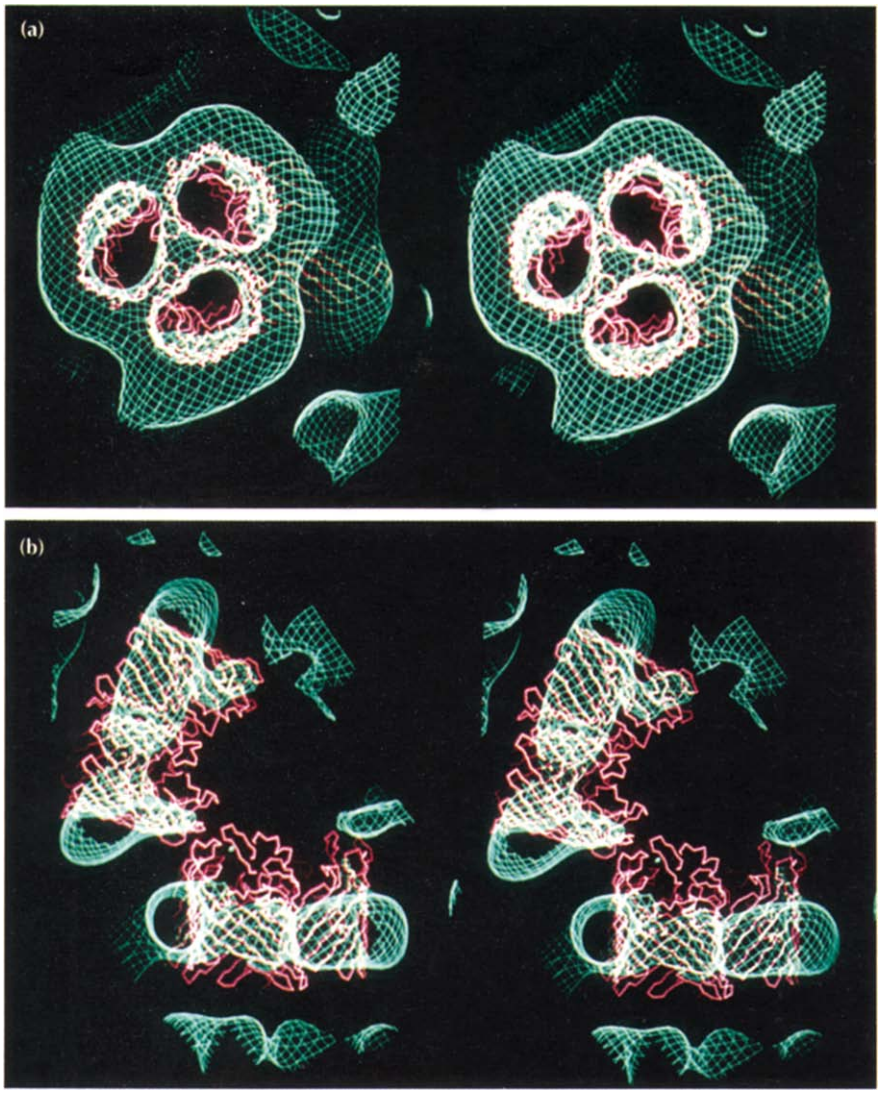

Fig. 3. Stereoviews of the scattering-length density map of βOG–porin at 100% D_2O where both protein and detergent should be visible at negative contrast. Any part of the detergent forming a condensed non-hydrated phase (e.g. the hydrophobic tails) should have a higher average contrast than the protein. The maps are contoured so as to enclose 20% of the unit cell volume. Therefore, the hydrophobic tails are the main features. **(a)** View parallel to the trimer threefold axis. **(b)** View perpendicular to the threefold axes of two trimers. Note how very similar the detergent belts are in Figures 2 and 3.

occupying 20–24% and 15–18% of the unit cell for C_{10}DAO and βOG respectively. This corresponds to 25–30% occupation of the unit cell by whole detergent molecules (head plus tail).

Five cycles of phasing were carried out for both the C_{10}DAO and βOG structures. The final model for C_{10}DAO–porin consists of 4% non-hydrated head groups and 20–24% hydrophobic tails. The volume of head groups modeled is consistent with the volume of tails. For the βOG crystals, no density which could have been interpreted as the head groups was seen at any D_2O concentration. Furthermore, the calculation of the R factors between observed and calculated structure factors for the whole model was lower when the scattering density of the detergent regions was assumed to correspond to that of βOG tails rather than to whole βOG molecules. This confirms that the modeled density primarily arises from the hydrophobic tails. The final model includes 15–18% of the volume of the unit cell. The improvements in the R factors during the modeling process are summarized in Table 1.

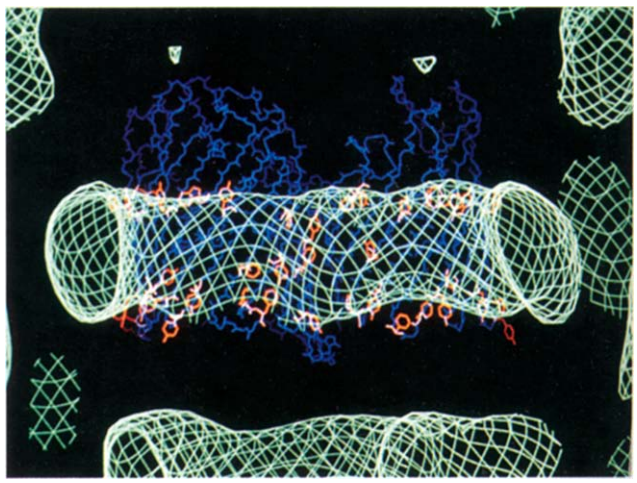

Fig. 4. The modeled detergent in the βOG–porin complex viewed perpendicular to the trimer threefold axis. The hydrophobic tails of the detergent (green density) fit exactly into the area delimited by the rings of aromatic side chains (red) at the hydrophobic/polar boundaries that probably correspond to the limits of the acyl chains of the lipid membrane. The porin polypeptide backbone is shown in blue.

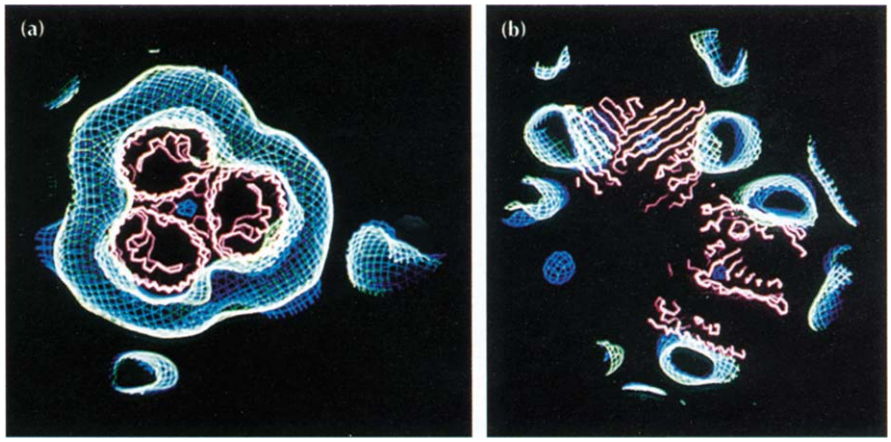

Fig. 5. A view of the modeled detergent belts for C_{10}DAO–porin (blue) and βOG–porin (green) showing that they superimpose almost exactly. **(a)** View parallel to the trimer threefold axis. **(b)** View perpendicular to the threefold axes of two trimers.

Detergent–protein interactions

The detergent regions can be modeled roughly as hollow cylinders around the porin trimer, defined by an internal radius R1 of 38 Å (equal to the radius of the protein trimer), an external radius R2 and a height of 25–28 Å. We find R2 has the value 58 Å for C_{10}DAO and 53 Å for βOG. From the relative volumes of head groups and tails (Table 1 in [12]) the radius, R3, delimiting the head group regions (using a simple cylindrical description) can be estimated. This indicates that the head groups form a shell around the tails with a thickness of 4 Å for C_{10}DAO and 9 Å for βOG. The limited resolution of the data (16 Å) makes it unlikely that the C_{10}DAO head groups could be seen unless they are non-uniformly distributed around the tails. This premise is consistent with the few patches of density observed around the trimer. Based on the volumes of the detergent belts, the number of detergent molecules per porin trimer is estimated to be approximately 410 C_{10}DAO molecules or 350 βOG molecules. No estimates exist for the number of C_{10}DAO or βOG molecules associated with porin in solution, but it has been shown that 180 molecules of the non-ionic detergent C8E4 are bound to porin in solution at 6°C and 310 molecules of C8E4 are bound at 29°C [17]. The X-ray structure of porin [5,10] shows two distinct rings of aromatic residues located around the trimer and separated by 25 Å, comprising mainly tyrosines and phenylalanines. It has been postulated that these 'aromatic rings' anchor the protein in the lipid membrane. Figure 4 shows how the modeled detergent density (in this case βOG) is exactly delimited by these rings of aromatic residues, confirming their role in defining a hydrophobic boundary on the surface of the protein. The thickness of the detergent belt (~25 Å) is very similar to that of the hydrophobic part of a lipid bilayer. The head groups presumably form hydrophilic interactions with bands of polar residues on either side of the hydrophobic zone. The density observed in the X-ray structure close to Tyr157 [10] and interpreted as an ordered detergent molecule does indeed

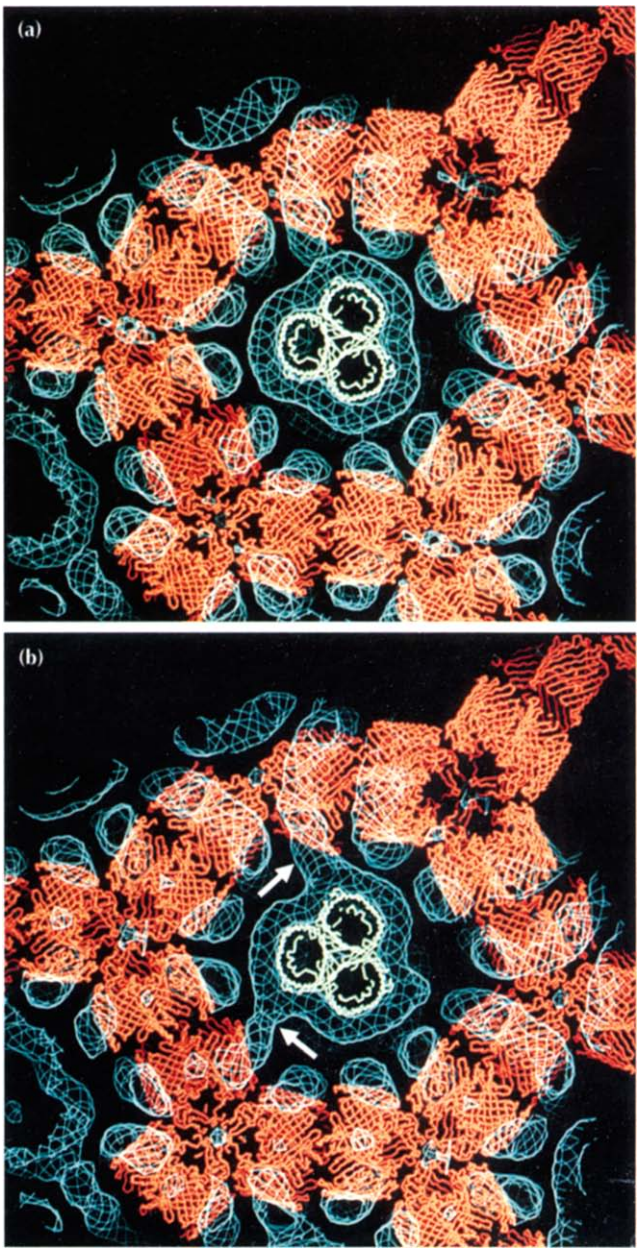

Fig. 6. Views of the packing of the detergent–porin complexes in the unit cell. There are no direct protein–protein contacts between the interpenetrating lattices shown in red and green. **(a)** The C_{10}DAO–porin complex. There are no visible contacts between detergent micelles indicating that interactions are probably through low contrast head group/head group contacts. **(b)** The βOG–porin complex. Interactions between the independent lattices are visible (shown by white arrows) and are probably mediated by the detergent head groups.

fall within the detergent density in the neutron maps. Interestingly, aromatic residues in the central part of the trimer also create hydrophobic contacts which may play a large part in stabilizing the trimers. The location of the detergent belts in C_{10}DAO-containing and βOG-containing porin crystals is strikingly similar (Fig. 5).

Crystal packing

Another significant question concerning the tetragonal porin crystal form relates to the forces underlying the cohesion of the crystal. The tetragonal form consists of chains of trimers associated tetrahedrally (through interactions between the loops that protrude from the β barrel core of the monomers) and forming a diamond-like lattice [10]. Within one tetrahedron, the interactions are through the long loops on the 'rough' side of the barrel, and between tetrahedra, the interactions are mediated by the short loops (or turns) on the 'smooth' side. There are two symmetry-related and interpenetrating lattices of tetrahedra in the unit cell and no protein–protein contacts are found between them. The cohesion of the crystal therefore must depend on favorable detergent–detergent interactions as well as protein–protein interactions. Figure 6 shows the protein–protein, detergent–detergent and protein–detergent interactions in the crystals. There does not appear to be a continuous detergent phase inside the crystal for the C_{10}DAO–porin complex (Fig. 6a) and no hydrophobic interactions are observed between the detergent surrounding one trimer and its stacked neighbor. However, the distance between two adjacent hydrophobic rings surrounding trimers in the independent lattices of tetrahedra (10 Å for C_{10}DAO and 15 Å for βOG) is consistent with the occurrence of interactions between the detergent head groups. In the case of βOG there seem to be a few, somewhat tenuous, interactions between detergent rings in adjacent independent chains of tetrahedra (Fig. 6b). Even though these interactions appear tenuous and are between spatially disordered molecules, they are sufficient to stabilize a crystal which diffracts X-rays to high resolution. The temperature sensitivity of the crystals (see the Materials and methods section) may well arise from the detergent head group interactions.

Biological implications

Little is known about the physics and structural interactions of lipids and proteins on a molecular scale. While crystal structures of membrane proteins have provided detailed information concerning the zones that form the interfaces between proteins and the lipid bilayer phase, direct observation of lipid–protein interactions has not yet been possible. The visualization of detergent domains around membrane proteins using single-crystal neutron diffraction provides information, albeit indirect, about the nature of these interactions.

We have used neutron diffraction to study the detergent-covered surface of the OmpF porin trimer, an integral membrane protein of the *Escherichia coli* outer membrane. Using two different detergents, we have demonstrated the formation of a detergent belt (~25 Å high) around the porin trimer. This belt is very similar to that found for two photosynthetic reaction centers. Moreover, we have shown that the rings of aromatic residues (mainly tyrosine and phenylalanine) postulated to delimit the detergent-binding zone, clearly fulfill this role in porin. Similar, though less pronounced, bands of aromatic residues delimiting the detergent-binding zone are present in the photosynthetic reaction centers. They may play a less significant role in reaction centers which interact not only with lipids but also mainly with other proteins (e.g. light-harvesting complexes).

The OmpF crystal structure also highlights the contribution of the interactions between detergent head groups in the formation and stability of these membrane protein crystals. In reaction center crystals it appears that polar protein–protein interactions are the major contributors to crystal integrity although detergent–detergent interactions may play a role in stabilizing the crystal structure. Fusion of detergent layers, as evidenced by continuous hydrophobic domains, does not seem to play a significant role in crystallization of the OmpF porin, at least not in the tetragonal crystal form.

Materials and methods

Protein purification and crystallization

OmpF porin was purified from the B^E strain of *E. coli* as described previously [18].

Crystals for neutron diffraction were grown from solutions containing 0.9% β-octyl glucoside (βOG), 0.1 M sodium phosphate and 0.09% C8E6-11 using 13.5% PEG2000 as a precipitant [9] except that the aqueous phase consisted of various mixtures of either 0, 25, 60 or 100 mole percent D_2O/H_2O. These crystals were either used as such or the β-octyl glucoside was replaced by d_{10}-decyl-*N,N'*-dimethyl amine oxide (tail-deuterated C_{10}DAO). Crystals do not suffer damage due to neutron irradiation.

βOG crystals: Preliminary experiments had shown that the crystals were rather sensitive to temperature during transport or during the rather long time (4–10 days) of data collection. This problem was overcome by cross-linking the crystals with 0.1% gluteraldehyde. The only apparent effect of this cross-linking was to reduce the observable resolution limit (as judged by X-ray diffraction) to 5–7 Å, outside the limit of the neutron data. Cell dimensions were unchanged as measured by X-rays: a=b=154 Å, c=172 Å, space group $P4_2$.

C_{10}DAO crystals: Crystals containing d_{10}-C_{10}DAO (deuterated decyl chain, hydrogenated amino methyl groups) were prepared in order to enhance the contrast between detergent and protein. This was done by soaking βOG crystals for one week in two changes of solutions containing the same constituents

as the βOG crystals but instead of βOG substituting d_{10}-C_{10}DAO and 0, 35, 70 or 100% D_2O/H_2O as the aqueous phase. The exchange of detergent molecules could be monitored by following the birefringence in the crystals, which is normally low due to their nearly cubic arrangement. However, during the detergent exchange the birefringence increased and disappeared again as the exchange was accomplished. (The d_{10}-C_{10}DAO was a kind gift of Dr Hartmut Michel and Dr Michel Roth.)

The D_2O content of the crystals was checked by neutron transmission measurements of the mother liquor from which the crystals were taken. Crystals of maximum dimension 0.5 mm were mounted in quartz capillaries as for X-ray diffraction, except that a small indentation in the tube was made to avoid slipping of the crystal in its low surface tension mother liquor during the exposure.

Data collection

Data from the crystals containing the different detergents were collected at different times and on two different instruments at the High Flux Reactor of the Institut Laue-Langevin, Grenoble, France. Throughout data collection the crystals were maintained at 18°C to eliminate the risk of the mother liquor composition changing by evaporation of the aqueous phase.

βOG crystals: Diffraction data were measured on the small-angle scattering instrument D17, modified for use as a single crystal diffractometer [19]. Neutrons were monochromated by a helical slot velocity selector giving an incident wavelength (λ) of 11.0 Å. The neutron detector was placed 810 mm from the crystal with its center offset at an angle of 22° to the incident beam. In this way data could be collected to a maximum resolution (minimum d-spacing) of 16 Å. Data were collected in normal beam geometry with steps of 0.1° in ω and stored on the instrument computer for off-line data reduction. Typical exposure times ranged from 5 min per 0.1° step (for high contrast, low background) to 20 min (for low contrast, high background). Four data sets were collected, with different D_2O concentrations in the solvent: 0, 25, 60 and 100% D_2O.

C_{10}DAO crystals: Neutron diffraction data for the C_{10}DAO–porin crystals were collected on the instrument DB21, which is a 4-circle diffractometer designed for low-resolution crystallography of large macromolecular assemblies [19]. The neutron wavelength was fixed at 7.53 Å by reflection from a K-intercalated graphite monochromator. The sample to detector distance was 250 mm. Data were collected in normal beam geometry with steps of 0.15° in ω. Typical exposure times ranged from 10–16 min per 0.15° step. Four data sets were collected at 16 Å resolution, with different D_2O concentrations in the solvent: 0, 35, 70 and 100% D_2O.

Data reduction

The orientation matrix and the first refinement of cell parameters and camera constants (crystal to detector distance, detector center) were determined using an interactive graphics program (KEA; P Metcalf, unpublished program). Data reduction was carried out using a package in which the reflection profile is predicted using the known instrument resolution function and an empirically derived mosaic spread for the crystal [20]. The internal agreement factors R_{sym}, the completeness and the number of unique reflections for each contrast and each type of crystal are summarized in Table 2.

Scaling of the different data sets

The diffraction intensities resulting from a contrast variation experiment show a parabolic variation with contrast for acentric reflections, and for centric reflections the structure amplitude (the square root of the intensity) shows a linear variation with contrast [21]. This property is used to scale together the four data sets, based on a least-squares technique [22]. However, in space group $P4_2$ reflections of the types hkl and khl are not equivalent and it is therefore necessary to ensure that data sets from different crystals and, in our case, crystals of different contrast, have the same hand. In order to do this we exploited the linear variation with contrast of centro-symmetric structure factors. Thus, we scaled together data sets at different contrasts using only those centro-symmetric reflections that are independent of hand, that is, the hh0 and h00 reflections. Then defining arbitrarily the hand for one contrast (say 0% H_2O/D_2O), we examined which combinations of hand produced a linear variation of structure factor for other centro-symmetric reflections of the type hk0. In principle, once the hand is fixed for one pair of reflections of the type (hk0, kh0) then that of the whole data set is determined. In practice, it was necessary to examine several reflections as structure factors that are weak in

Table 2. Experimental data collection statistics at 16 Å resolution.

Detergent	D_2O content (%)	Total number of reflections	Number of unique reflections	Number of unique reflections >3σ	Completeness of data (%)	R_{sym}* (I>3σ)
β-OG						
	0	858	495	347	91.1	0.051
	25	1201	535	346	98.5	0.049
	60	880	521	365	95.9	0.053
	100	897	504	431	92.8	0.032
C_{10}DAO						
	0	1148	482	292	88.7	0.032
	35	1206	515	297	94.8	0.034
	70	1214	514	291	94.6	0.042
	100	1193	514	258	94.6	0.033

Diffraction data were collected for several contrasts (i.e. several D_2O concentrations of the solvent). *R_{sym} is defined as $\Sigma|I-\langle I\rangle|/\Sigma I$, where I is the intensity of an individual reflection, and $\langle I\rangle$ is the average over symmetry-related reflections. The R_{sym}s are calculated over the whole resolution range. As a function of resolution (d), R_{sym}s vary typically from 2.5% (d>30 Å) to 7% (20 Å<d<30 Å) and 14% (d<20 Å) for reflections with I>3σ.

one contrast could produce ambiguous choices of hand. The choice of hand was also checked by scaling together the data sets for all combinations of hand. From the scaled data sets interpolated structure factors (F_{calc}) could be obtained and an agreement factor between observed and calculated structure factors obtained for each combination of hand. The agreement factor between the observed and the fitted values was significantly lower for the correct combination (6% compared with a range of 14–29%). Once the same relative hand had been chosen for all four contrasts, the data sets were scaled together using both the linear relationship between centro-symmetric structure factors and the general quadratic relationship between general structure factors.

Structure determination

Contrast variation: Neutron contrast variation experiments give the differences in phase between structure factors measured at different contrasts [23]. The determination of the absolute phases requires the introduction of supplementary information. The procedure followed here was to calculate the phases according to the BESF algorithm developed by Roth [24]. A starting partial model was obtained from the protein coordinates determined by X-ray crystallography at 3 Å resolution [10]. The first step was to determine the H_2O/D_2O concentration at which the detergent made a minimum contribution to the observed data. This was done by comparing the observed structure factors, F_{obs} (obtained for any H_2O/D_2O content by interpolation from the experimental data using the parabolic variation of the diffracted intensities with contrast), with the structure factors (F_{calc}) calculated considering the protein contribution only. The best agreement (minimum R factor; $R=\Sigma|F_{obs}-F_{calc}|/\Sigma F_{obs}$) was found at 3% D_2O in the case of βOG and at 110% D_2O in the case of C_{10}DAO. The latter figure has, of course, no physical meaning but is a virtual value extrapolated from the linear variation of scattering-length density with D_2O content of the water (Fig. 1). In both cases, these values are close to the match points of the hydrophobic tails of the detergent molecules rather than the whole detergent molecules (see Table 1 in [12]). This is a first indication that the hydrophobic part of the detergent dominates the neutron diffraction by forming large domains in the crystals. In the case of C_{10}DAO, the small volume occupied by the head groups relative to the tails results in regions that are probably too small, compared with the resolution, to be observed. In the case of βOG, we see from Figure 1 that the match point of the glucoside head groups is at about 50% D_2O. The variation, however, of the scattering-length density of the head group as a function of H_2O/D_2O ratio, is not very different from that of the solvent scattering density. As a result, the contrast of the head groups is never very large relative to the contrast of the hydrophobic tail. In addition, the head groups are likely to be hydrated, and although this effect will not change the match point, it will modify the slope of the scattering density and decrease the contrast at all D_2O concentrations. It has been estimated that, for example, in C_{12}DAO there are approximately three water molecules per head group [24].

Model building

C_{10}DAO: The C_{10}DAO–porin complex was modeled first. The protein model derived from the X-ray study [10] was used to calculated the phases at 110% D_2O concentration. This phase set was used as a starting point. In the first cycle, centroid phases at 19, 40 and 110% D_2O concentration were estimated from the contrast-variation relationships and scattering-length density maps produced. The detergent regions were identified considering that they comprised a given volume fraction of the unit cell and then modeled as follows. Hydrophobic tail regions and head group regions were defined. The complete resulting models (protein+tails+head groups) were used to calculate structure factors at 0, 35, 70 and 100% D_2O. The moduli of the structure factors were compared with the observed ones and the resulting R factor was used as a test for the validity of the model. These phases were input into the BESF algorithm to generate new phases and calculate new density maps to be modeled. A flow chart of the procedure is shown in Figure 7. Convergence of the cycling procedure was monitored through the R value.

The hydrophobic tail regions were modeled from the 19% D_2O or the 40% D_2O maps. A concentration of 40% D_2O corresponds to the match point of the protein and the contribution of head groups is negative. A concentration of 19% D_2O corresponds to the match point of the head groups and the contrast of the tails is higher than at 40%. Both of these concentrations have their advantages and disadvantages: it is, therefore, interesting to consider both of them (the densities which are not common to the two maps might be considered as noise). For each model building exercise, the protein density, the location of which is already known, was masked in the map so that it was not considered in the detergent modeling. It is known from the amino acid sequence that the protein occupies 26% of the total volume in the unit cell. The protein mask was calculated from the protein coordinates with

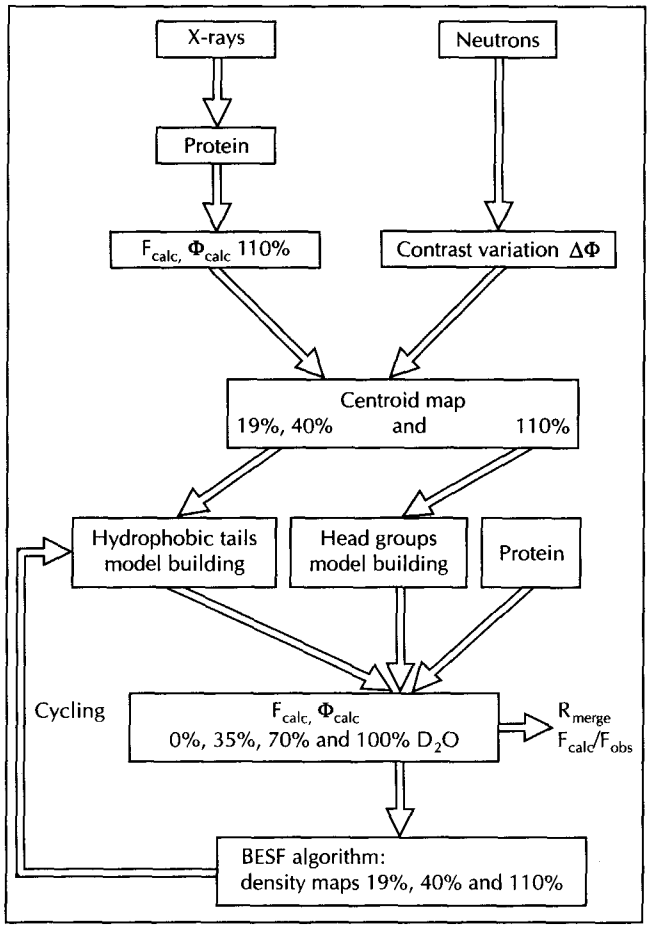

Fig. 7. Flow chart summarizing the detergent model building for C_{10}DAO. A similar procedure was used for β-OG.

a solvent of 110% D_2O. The detergent volume fraction in the crystal is not known accurately, although Garavito *et al.* [9] estimated it to be between 20% and 36% of the cell volume using radioactive labeling studies. A first estimate was made, by examination of the maps (at 19% or 40% D_2O concentration) at different density levels and deciding at which level the density became merely noise. The stability of the density assigned as detergent from one cycle to the next, or consistency between the 19% and the 40% D_2O maps in the same cycle were also important criteria. This density level corresponded to a volume of hydrophobic tails of about 20–24%. The density can be smoothed before modeling, then after masking out the protein density, the highest density regions (corresponding to a volume of about 20%) were modeled as hydrophobic tails. The map smoothing was done only in the first cycle over a radius of 8 Å. The modeled density was then transformed into pseudo-atoms. For subsequent structure-factor calculations, the scattering density of these atoms were the scattering densities of the hydrophobic tails. The volume of the modeled density can also be adjusted by following the agreement factors between observed and calculated structure factors at 40% D_2O. However this criterion turned out not to be sufficiently sensitive. In the last two cycles, the volume of the tails was not modeled in one step. First, 20% of the volume was modeled defining a partial but almost complete model of tails. Then, small volumes of tails (2%) were added step by step, by modeling difference Fourier maps, F_{obs}–F_{calc} (protein+partial tail model). In each step, the excluding mask had to be adjusted in order not to model the same regions twice. This method gave significant improvements on the modeling as seen in the improvement of the R factors between intermediate and final models (Table 1).

Although the volume of the head groups in C_{10}DAO is small, their contribution is not negligible as seen in the R factor at 110% D_2O (Table 1). Furthermore, in the first 110% D_2O density map calculated with centroid phases, small high-density bubbles, which are not due to the protein, were present around the protein at 15–18 Å from the surface. In parallel to the tail modeling, at each cycle the head groups were modeled from difference Fourier maps, F_{obs}–F_{calc}, in a similar way to the tail regions, adding small volumes (2%) step by step.

βOG: For βOG–porin, starting phases were calculated from the protein component alone at 3% D_2O (which is the match point of the detergent) and 100% D_2O (a concentration at which the contributions of protein and detergent to the diffraction are similar). The additional phase information coming from the protein structure in 100% D_2O allows best phases [23,25], rather than centroid phases, to be subsequently employed. The first 40% D_2O map showed a density quite similar to the hydrophobic tail region modeled for C_{10}DAO–porin. For this reason it was decided to shorten the cycling procedure: the phases at 3% and 100% D_2O were calculated using the protein and this βOG tail model. The tails were modeled from the 40% or the 100% D_2O maps, in the same way as described for C_{10}DAO. Although the 40% D_2O concentration corresponds to the protein match point, the 100% D_2O map was easier to model because of a better contrast for the hydrophobic tails and a less noisy map.

Acknowledgements: We thank Sandra Cowan and Tilman Schirmer for providing the atomic coordinates of tetragonal porin prior to publication and Michel Roth for helpful discussions.

References

1. Deisenhofer, J., Epp, O., Miki, K., Huber, R. & Michel, H. (1985). Structure of the protein subunits in the photosynthetic reaction centre of *Rhodopseudomonas viridis* at 3 Å resolution. *Nature* **318**, 618–624.
2. Arnoux, B., *et al.*, & Chang, C.H. (1989). Structure of spheroidene in the photosynthetic reaction center from Y *Rhodobacter sphaeroides*. *FEBS Lett.* **258**, 47–50.
3. Weiss, M.S., *et al.*, & Schulz, G.E. (1991). The structure of porin from *Rhodobacter capsulatus* at 1.8 Å resolution. *FEBS Lett.* **280**, 379–382.
4. Kreusch, A. & Schulz, G.E. (1995). Refined structure of the porin from *Rhodopseudomonas blastica*. Comparison with the form from *Rhodobacter capsulatus*. *J. Mol. Biol.* **243**, 891–905.
5. Cowan, S.W., *et al.*, & Rosenbusch, J.P. (1992). Crystal structures explain functional properties of two *E. coli* porins. *Nature* **358**, 727–733.
6. Schirmer, T., Keller, T.A., Wang, Y.-F. & Rosenbusch J.P. (1995). Structural basis for sugar translocation through maltoporin channels at 3.1 Å resolution. *Science* **267**, 512–514.
7. McDermott, G., *et al.*, & Isaacs, N.W. (1995). Crystal structure of an integral membrane light-harvesting complex from photosynthetic bacteria. *Nature* **374**, 517–521.
8. Garavito, R.M. & Rosenbusch, J.P. (1980). Three-dimensional crystals of an integral membrane protein: an initial X-ray analysis. *J. Cell Biol.* **86**, 327–329.
9. Garavito, R.M., Jenkins, J., Jansonius, J.N., Karlsson, R. & Rosenbusch, J.P. (1983). An X-ray diffraction analysis of an integral membrane protein: porin from *E. coli*. *J. Mol. Biol.* **164**, 313–327.
10. Cowan, S.W., *et al.*, & Schirmer, T. (1995). The structure of OmpF porin in a tetragonal crystal form. *Structure* **3**, 1041–1050.
11. Zulauf M., Timmins P.A. & Garavito R.M. (1986). Neutron crystallography of a membrane protein. Localization of detergent and protein at 20-Å resolution. *Biophys. J.* **49**, 96–98.
12. Timmins, P.A., Pebay-Peyroula, E. & Welte, W. (1994). Detergent organisation in solution and in crystals of membrane proteins. *Biophys. Chem.* **53**, 27–36.
13. Roth, M. (1991). Phasing at low resolution. In *Crystallographic Computing*. (Moras, D., Podjarny, A.D. & Thierry, J.C., eds), vol. **5**, pp. 229–248, Oxford University Press.
14. Timmins, P.A. & Zaccai, J. (1988). Low resolution structures of biological complexes studied by neutron scattering. *Eur. Biophys. J.* **15**, 257–268.
15. Roth, M., Lewit-Bentley, A., Michel, H., Deisenhofer, J., Huber, R. & Oesterhelt, D. (1989). Detergent structure in crystals of a bacterial photosynthetic reaction centre. *Nature* **340**, 659–662.
16. Roth, M., Arnoux, B., Ducruix, A. & Reiss-Husson, F. (1991). Structure of the detergent phase and protein–detergent interactions in crystals of the wild-type (strain Y) *Rhodobacter sphaeroides* photochemical reaction center. *Biochemistry* **30**, 9403–9413.
17. Zulauf, M. (1985). Interactions of nonionic detergents with membrane proteins: solubilization and crystallization of protein–detergent complexes. In *Physics of Amphiphiles: Micelles, Vesicles and Microemulsions. Proceedings of the International School of Physics "Enrico Fermi"*. (Degiorgio, V, and Corti, M., eds), pp. 663–673, North Holland Press, Amsterdam, Oxford, New York, Tokyo.
18. Garavito, R.M. & Rosenbusch, J.P. (1986). Isolation and crystallization of bacterial porin. *Methods Enzymol.* **125**, 309–328.
19. *Guide to Neutron Research Facilities at the ILL*. (1994). Available on request from ILL, BP 156, 38042 Grenoble Cedex 9, France.
20. Roth, M. & Lewit-Bentley, A. (1982). Low resolution neutron diffractometry with a position-sensitive multidetector. *Acta Cryst. A* **38**, 670–679.
21. Worcester, D.L. (1976). Neutron beam studies of biological membranes and membrane components. In *Biological Membranes*. (Chapman, D. & Wallach, D.F.H., eds), vol. **3**, pp. 1–46, Academic Press, London.
22. Roth, M., Lewit-Bentley, A. & Bentley, G.A. (1984). Scaling and phase difference determination in solvent-contrast variation experiments. *J. Appl. Cryst.* **17**, 77–84.
23. Roth, M. (1987). Best density maps in low-resolution crystallography with contrast variation. *Acta Cryst. A* **43**, 780–787.
24. Timmins, P.A., Leonhard, M., Weltzien, H.U., Wacker, T. & Welte, W. (1988). A physical characterization of some detergents of potential use for membrane protein crystallization. *FEBS Lett.* **238**, 361–368.
25. Blow, D.M. & Crick, F.H.C. (1959). The treatment of errors in the isomorphous replacement method. *Acta Cryst.* **12**, 794–802.

Received: **26 Jun 1995**; revisions requested: **24 Jul 1995**; revisions received: **14 Aug 1995**. Accepted: **15 Aug 1995**.